

NONLINEAR CURRENT-VOLTAGE CHARACTERISTICS DUE TO ION MIGRATION IN LOW-DIMENSIONAL ORGANIC METAL HALIDE HYBRIDS

Meg Van Deventer



Margaret (Meg) Lydia van Deventer is a senior at Florida State University completing a Bachelor of Science in Physics with minors in English and Math. Margaret performs research with Dr. Peng Xiong, a professor and researcher of condensed matter in the Physics department.

Abstract

Perovskite-related metal halide hybrids are currently a hot topic in materials research because of their affordability, efficiency, and abundance. Rapid advances are being made in terms of improving the performance of perovskite-based photovoltaics, but the materials remain unstable in the presence of light, moisture, and heat. A more comprehensive understanding of the physical processes of these materials is necessary for us to make improvements to the stability and efficiency of organic metal halide hybrids. Specifically, much research in this field focuses on higher-dimensional (2D, 3D) structures. Lower-dimensional materials (1D and 0D) may provide more stability by virtue of their molecular structures but require further investigation. One issue that is particularly relevant to stability is ion migration in these materials, in which mobile ions move as a result of an applied electrical bias and induce an electric field that opposes said bias. This research examines data taken from several lower-dimensional samples while they are exposed to a light source in order to gain a deeper understanding of the electrical transport properties of N,N'-dimethylethylenediaminium tin iodide ($C_4N_2H_{14}SnI_4$). In particular, we will examine the effect that ion migration may have on the current-voltage characteristics of $C_4N_2H_{14}SnI_4$.

Keywords: perovskites, solar, condensed matter, photovoltaics, physics

NONLINEAR CURRENT-VOLTAGE CHARACTERISTICS

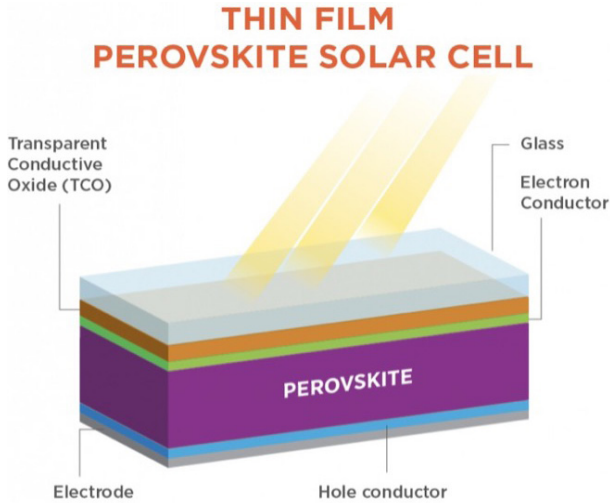
Low-dimensional organic perovskite-related metal halide hybrids are currently a popular research subject in materials science because of their many interesting optoelectronic properties, which suggest promising applications in devices such as solar cells, LEDs, and photodetectors (Liu et al., 2019). These materials have generated interest because they are cheap, abundant, and effective - three qualities that have led some scientists to refer to perovskites as the 'holy grail' of solar cell materials.

In the field of solar energy, it is possible to substitute perovskite metal-halide hybrids for silicon, a semiconductor currently used in over 90% of solar cells on the market ("Perovskite Solar Cells"). Because of perovskite's band gap tunability, it would also be possible to increase the efficiency of current solar cells by using silicon and perovskites in tandem, as perovskites can complement the absorption of whatever substance they are in tandem with ("A History of Perovskite Solar Cells", 2018). Solar cells are formed by a semiconductor layer, known as the absorber layer, that sits between an electron conducting layer (n-type semiconductor) and a hole conducting layer (p-type semiconductor). When the sun's rays strike the solar cell, incoming photons excite electrons in the absorber layer and create free electron-hole pairs known as excitons. These electrons and holes travel along a transport pathway composed of the electron and hole conducting layers and the absorbing layer, and said current is gathered by an electrode.

Silicon solar cells are limited by high cost as well as physical fragility, which makes them difficult to transport. Additionally, perovskite solar cells have achieved conversion efficiencies of up to 25.2% in 2019 (up from 3.8% in 2009) (Vekony, 2020). The current efficiency record for a silicon solar cell is currently 26.7%. While this is higher than 25.2%, it has taken decades to reach this level of efficiency, and research suggests that we are approaching the efficiency limit of silicon("Perovskite Solar Cells"). This implies that with time and research, perovskite based solar cells have the potential to become significantly more efficient and widely available than those made with silicon.

That being said, perovskite solar cells are not yet market-ready because of the substance's susceptibility to moisture, light, and heat. Because they deteriorate so quickly, research must be done to make them more resilient before they become a viable substitute for silicon. Several attempts to improve perovskite solar cell stability have included cell encapsulation, the use of buffer layers, and the optimization of perovskite compositions(Liu et al., 2019). In general, these attempts have been concentrated on two-dimensional (2D) and three-dimensional (3D) perovskites. Our research focuses on the behavior of low-dimensional halide perovskites, in which the metal-halide chains are

Figure 1: Components of a perovskite solar cell. Source: U.S. Department of Energy



insulated by a protective organic cation layer, suggesting that they may be more resilient against environmental factors than their higher-dimensional counterparts (Ma et al., 2019).

One phenomenon that must be understood in order to make advances in perovskite-hybrid technology is the appearance of current-voltage (I-V) hysteresis. When I-V measurements are performed on perovskite samples, hysteresis makes it difficult to accurately analyze or reproduce results (Liu et al., 2019). Hysteresis is also often exaggerated in the presence of a light source (Liu et al., 2019). Several hypotheses for this phenomenon have been offered, including the ferroelectric effect, unbalanced charge carrier transport or ion and ion vacancy migration. This research concentrates on the latter, and the effect that it may have on charge transport in metal halide hybrids.

The purpose of this research is to gain a deeper understanding of the effect that light has on field-assisted ion and ion vacancy migration within metal halide hybrids. This includes identifying which ions may be responsible for the induced electric field, how their motion relates to the bias current, and how many ions may be accumulating at each side of the crystal to induce said electric field.

This thesis is organized into a background, which will give information on metal-halide hybrids as well as field-assisted ion migration. Next, we will describe the experimental methods used to gather our data and present said data. After that, we will present analysis performed on the data gathered over the course of our research. Finally, the findings are summarized into a conclusion and the future of this research is discussed.

Background

Metal-Halide Hybrids

Perovskite is a classification that refers to both the mineral calcium titanate and a class of materials that share the same structure as calcium titanate. While perovskite was discovered in 1839 by mineralogist Gustav Rose, it was mainly used for pigmentation until the discovery of barium titanate in 1945. The substance is named for Lev von Perovski, a Russian nobleman and mineralogist (“A History of Perovskite”, 2018).

The classic perovskite structure can be written as ABX_3 , where A and B are cations of varying size and X is an anion. ABX_3 has a body centered cubic (BCC) structure, visible in figure 2.

Figure 2: Perovskite unit cell with BCC structure.

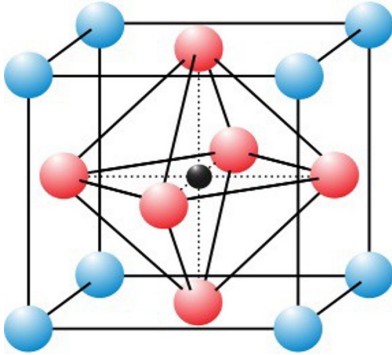


Fig. 2 If we consider the ABX_3 perovskite structure, the blue spheres are the A ions (cations), the red spheres are the B ions (also cations), and the small black sphere at the center is X (an anion). Source: Wikimedia Commons

Metal-halide hybrids fall within the perovskite class but specifically contain a metal and a halogen. Several features, including a high absorption coefficient, ease of tunability and direct band gap make these materials extremely promising for photovoltaic applications.

The most common metal-halide hybrids used in photovoltaic cell research are methylammonium lead iodide ($CH_3NH_3PbI_3$) based (Eames et al., 2015). While some of our research was initially performed with lead iodide, we found that because of the toxicity of lead it was easier to fabricate samples from tin iodide hybrids. Tin has a lone pair of valence electrons just like lead and is in the same periodic group, so it is an acceptable substitute that is already being used in some perovskite-related research (Kamminga et al., 2019). The crystals used in

this experiment are N,N'-dimethylethylenediaminium tin iodide ($C_4N_2H_{14}SnI_4$).

Low-dimensional metal-halide hybrids are of particular interest because of their chemical stability. Typically, the categorization "low-dimensional" can be employed to describe two different classes of perovskites: those with molecular-level low-dimensionality and those with morphological low-dimensionality. Morphologically low-dimensional metal-halides are compounds with physical low-dimensionality. This includes 0D quantum dots, 1D nanowires, and 2D nanoplatelets. Our research is focused on molecular-level low-dimensional metal-halide hybrids. In these measurements, we examined 1D $C_4N_2H_{14}SnI_4$ halide chains. These are formed by long chains of individual metal-halide molecules surrounded by a layer of organic cations. As discussed in the introduction, one of the main concerns surrounding perovskites is stability in the presence of external factors like moisture and heat. The protective layer of organic cations surrounding the unstable metal-halide species tells us that lower-dimensional metal-halides may be more stable than their higher-dimensional counterparts (Ma et al., 2019).

Field-assisted ion migration

Ion migration has frequently been proposed as one phenomenon that may be at fault for the hysteresis commonly found in current-voltage (I-V) data taken from perovskites (Wang et al., 2017). Ionic conduction has been well-documented in perovskite hybrids, both theoretically (Azpiroz et al., 2015) and confirmed experimentally using techniques such as temperature dependent photocurrent mapping (Wang et al., 2017). Additionally, a non-zero voltage shift observed at zero current within our own samples supports this possibility.

Before any bias is applied, mobile ions are distributed evenly across the sample. Once a bias is applied, ions and ion vacancies begin to travel along the applied electric field (E_{bias}) until they accumulate. The buildup of these ions and vacancies causes a separate induced electric field (Eion) that counteracts E_{bias} . Eion increases proportionally to E_{bias} until at some point the hole-current will no longer allow Eion to increase. Once this saturation point has been reached, the electric field that the sample is experiencing is simply the difference between E_{bias} and Eion. After the bias is removed, the relaxation period in which Eion returns to zero has been reported to be on the order of 10^2 seconds (Eames et al., 2015). In this case, it seems that the migrating ions may be Γ^- ions and their vacancies.

Additionally, it has been shown that photo illumination may have some minor enhancement of ion migration (Xia et al., 2019). More research must be done in this area as no definitive relationship between light and ion migration has been quantified or cemented.

NONLINEAR CURRENT-VOLTAGE CHARACTERISTICS

Methods

Synthesis and Fabrication

The crystals used in these measurements were synthesized by Dr. Qingquan He, a postdoctoral fellow in the Ma group of the Department of Biochemistry and Chemistry at FSU. In order to protect the samples from light and moisture, the synthesis took place on a Schlenk line reaction system with N₂ protection.

First, a mixture of 10 mL HI (57 wt. % in H₂O) and 1 mL H₃PO₂ (1 mL) was heated to 120° C and 0.5 mmol of Tin(II) iodide powder was dissolved in. This occurred under nitrogen flow and constant magnetic stirring for approximately 5 minutes. 0.5 mmol of N,N'-dimethylethylenediamine were then added, creating a clear solution. Once this clear solution was reached, magnetic stirring ceased and the solution was left undisturbed at room temperature overnight. During this rest period, the C₄N₂H₁₄SnI₄ crystals were able to form. These crystals varied from batch to batch in terms of surface roughness, color, length, and brittleness. An ideal crystal for our measurements needed to be long enough that we could fabricate four contacts on its surface and not so brittle that it would splinter during the fabrication process.

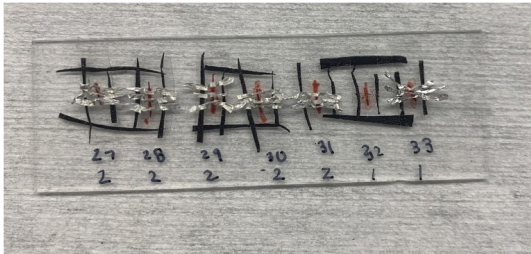
In order to avoid sample degradation from light and moisture, crystals were stored in a glovebox or vacuum system until measurements were taken. Additionally, synthesis was performed relatively close to when samples were prepared and measured.

To conduct electrical measurements on these samples, individual crystals were mounted onto glass slides using a small amount of exposed photoresist. In order to create contacts on the samples, thermal evaporation was performed to deposit 5 nm of Cr and 30 nm Au on the samples. To ensure that this process created four individual electrodes rather than simply depositing an uninterrupted layer of metal onto the sample, two types of shadow masks were used to disrupt the Cr/Au layer in three places. The first shadow mask was fabricated using thin strips of aluminum foil. The foil strips were manually laid above the crystal so that they were not in direct contact with its surface but were held in place by contact tape placed parallel to the crystal. This placement did not allow evaporated Cr/Au particles to reach the sample and created a set of four electrodes on the crystal. While this method allowed us to precisely select where the contacts were placed and control how many contacts were placed on a sample, it was time-consuming as the foil strips had to be extremely thin in order for the gold to evaporate in between strips. Additionally, the process of placing the aluminum foil on the samples presented a danger to some of the more fragile crystals, as it was easy to accidentally damage the surface while applying the foil strips to the contact tape. The second shadow mask was a prefabricated mask made of stainless steel

that could simply be placed over the sample, held in place by contact tape. This method took much less time and created electrodes that looked exactly the same every time but did not allow us much control over the number and placement of the electrodes.

Figure 3: Two different experimental methods used to create Cr/Au electrodes onto our samples.

3a. Aluminum foil strips



3b. Stainless steel shadowmask

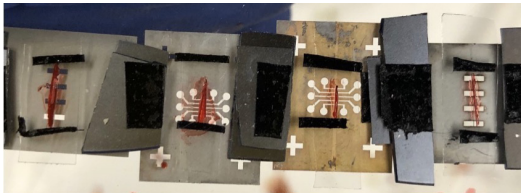


Fig. 3 This is how a sample looked right before it was placed into the evaporator.

After thermal evaporation, the glass slide and attached crystal were attached to an electrical socket with 14 pins, again using exposed photoresist. Silver contacts were then created on the surface of the crystal using silver paint and platinum wire. While it would have been possible to make electrical measurements on the samples using only silver paint and no gold evaporation, silver paint contacts have an inherently high contact resistance. The evaporated Cr allows the silver contacts to adhere to the sample more effectively and the Au mitigates the effect of the resistance of the silver paint on the total measured resistance of the sample. The platinum wire was then soldered with indium to pins on the socket.

NONLINEAR CURRENT-VOLTAGE CHARACTERISTICS

Figure 4: This picture is a fabricated sample underneath a microscope.

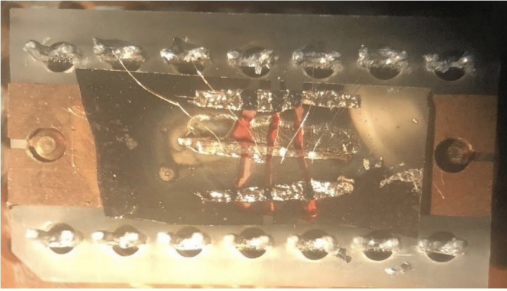


Fig. 4 Lining the top and bottom of the photo are the 14 pins that each contact is connected to by a thin platinum wire. The crystal itself is in the center of the sample. The three red lines are the areas where the aluminum foil mask prevented Cr/Au from evaporating onto the surface.

A total of four contacts were made on each sample. Because each crystal had a length on the order of a few millimeters, it was not productive to try and fit more than four on the sample with space in between each contact. Any less than four would prevent us from being able to neglect contact resistance in our data. With four contacts, we were able to run current across the contacts on each far end of the crystal and measure the change in voltage across the two middle contacts.

The data included in this thesis is from three crystals, all synthesized in the same batch. For this reason they are extremely similar in physical characteristics such as length, color, and surface roughness. The electrodes made on these samples were formed by an aluminum foil shadow mask.

Measurements

The electrical measurements on our samples were performed using a Keithley 2400 source meter and an HP 34401 multimeter. The setup of these two meters and sample can be seen in figure \ref{setup}. Beginning at -30 nA and increasing by increments of 3 nA until 30 nA was reached, a small current was applied from one contact at the far end of the sample to the contact at the opposite end (from here on, these two contacts will be referred to as the current leads). Two main types of measurements were taken on these samples. First, a control run was performed using two terminal (2T) measurements to make sure that the equipment was properly set up and the samples were intact. In this instance, voltage at each of the current leads was measured and the change in voltage between them was plotted against the applied current. Because the silver paint contacts have an inherently high resistance, this is a good way for us to make sure that our setup is working, but an inaccurate measurement as it

measures both the resistance of the sample and the contacts. To get a reading that only measured the resistance of the sample, we performed four-terminal (4T) measurements. Across the two middle contacts, the voltage at each contact (or voltage lead) was measured and the change in voltage between the two leads was calculated. The applied current and voltage drop between the leads was then plotted as an I-V curve.

Figure 5: This is a picture of our experimental setup, taken and labeled by Gillian Boyce.

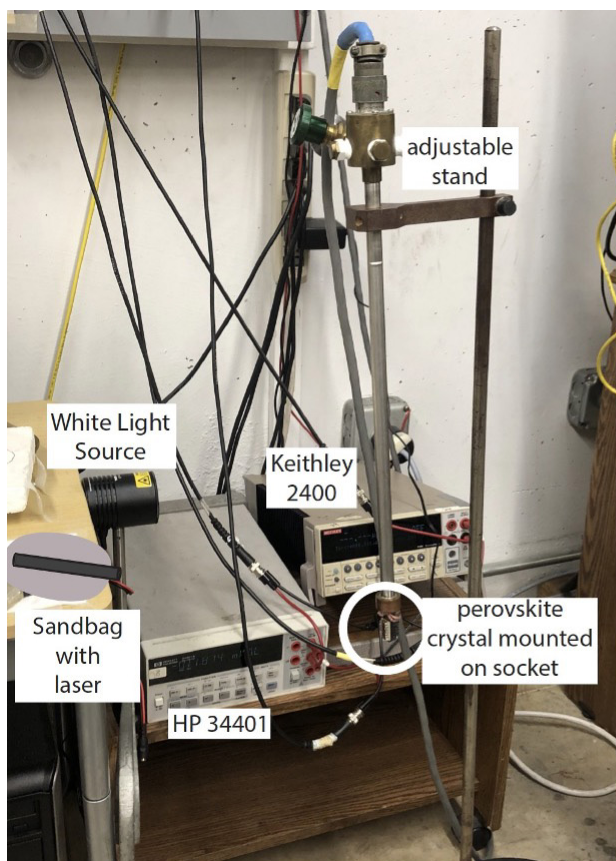


Fig. 5 The socket holding the fabricated sample is connected to the source meter and multimeter by the adjustable stand. On the desk adjacent to the meters is the white light source, and an illustration of how the laser is held in place by a sandbag.

In order to explore how light affected the photovoltaic characteristics of the

NONLINEAR CURRENT-VOLTAGE CHARACTERISTICS

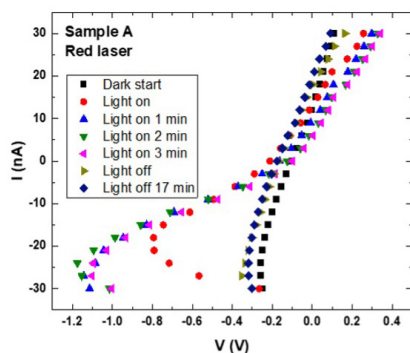
samples, we systematically applied a white light and several different colors of laser to the samples while taking measurements. We used lasers that were red, blue, and green (wavelengths 650, 405, and 532 nm respectively). Because of the small size of the samples, lasers allowed us to concentrate the beam of light directly onto the halide perovskites. The white light had a wider beam, but was still focused over the sample. One factor that can affect how the sample responds to light is exposure time, so a timer was used throughout these measurements to monitor how long the light had been applied or removed. First, a control measurement was made with no applied light source. As soon as the first -30 nA current was applied, we started a timer that kept going through the duration of the measurements. At 1 minute, the light source was turned on and current measurements began at the exact same time. This usually left about 30 seconds relaxation time in between measurements, where the light was not removed or added but no current was being applied to the sample. Measurements were then taken in 1 minute increments for several minutes of light exposure (usually 4 or 5), after which the light was turned off. A measurement was taken at the same time that the light source was removed. After 15 minutes of the sample having no light source placed on it directly, another measurement would be taken to see if any unique behaviors that occurred while the light source was applied were reversible.

Figure 6 shows the I-V measurements for three samples taken from the same batch. Each is experiencing a different monochromatic applied light source. This is the first run for each of these samples, meaning that they were held in vacuum until these measurements were taken and were not previously exposed to a focused light source like the lasers. Each graph has seven curves in total: the first taken with no applied light source, the next four taken with an applied light source, the sixth taken at the exact moment that the light source is removed, and the final taken approximately 15 minutes after the light source was removed and the sample has been left alone.

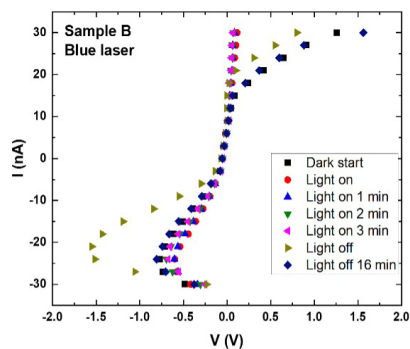
While these three samples have many differences in their data, several qualitative features are similar across the measurements. All of these samples exhibited a clear C-shape occurring at the beginning of the negative applied bias. This curve eventually disappears and is overtaken by a relatively linear I-V shape. That effect seems to increase in the presence of light and decreases eventually in its absence, with some exception. The presence of the C-curve is consistent with our hypothesis that field-assisted ion migration is occurring. Initially, negative ions and their positive vacancies are evenly distributed across the sample. As soon as the negative bias is applied, they begin to migrate, which causes the initial negative slope. At some point E_{ion} cannot increase

Figure 6: IV curves for three crystals from the same batch, each experiencing a different light source.

6a.



6b.



6c.

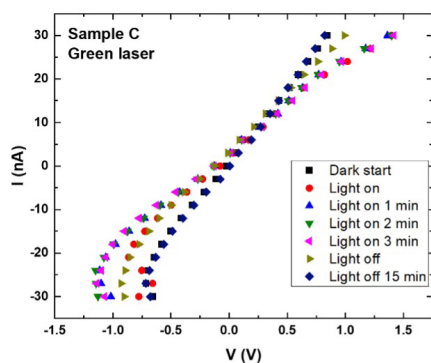


Fig. 6 This is the first run for these samples - in other words, it is the first time that we are testing their response to applied light. Typically, multiple runs were performed on each sample. However, the samples were extremely sensitive to both the current and applied light and deteriorated with each run.

any more, and the slope of the graph becomes positive as the primary source of current becomes charge carrier transport rather than ion migration. A graphical representation of this process is visible in figure 7.

Additionally, the slope (or resistance) of the quasi-linear section of graph that occurs immediately after the C-shaped curve consistently changed with exposure to light. However, the specifics of this change are inconsistent across samples. In sample A and C, the slope dramatically changed, but it increased under the blue laser (sample A) and decreased under the red (sample C). In sample B, we saw the resistance slowly and gradually decrease as light was applied, and then

NONLINEAR CURRENT-VOLTAGE CHARACTERISTICS

increase back to its initial point after the light was removed. Further research must be done to find out whether this is the result of the different light sources or simply a factor of the environment/fabrication.

In all three samples, the effects of illumination seem to be reversible. A final measurement was taken on each sample about 15 minutes after the light source was removed. For samples A and B, the I-V curve before light was applied and 15 minutes after light was applied are almost identical. For sample C, the curves are extremely similar, but the final curve is shifted approximately by approximately -0.05 V. The fact that these two curves exhibit similar (if not the same) C-curves supports the theory of ion migration, as previous work has shown that most ion induced fields have a relaxation period on the order of several minutes (Lee et al., 2019).

Figure 7: An drawing of an I-V curve with the characteristic initial c-shape.

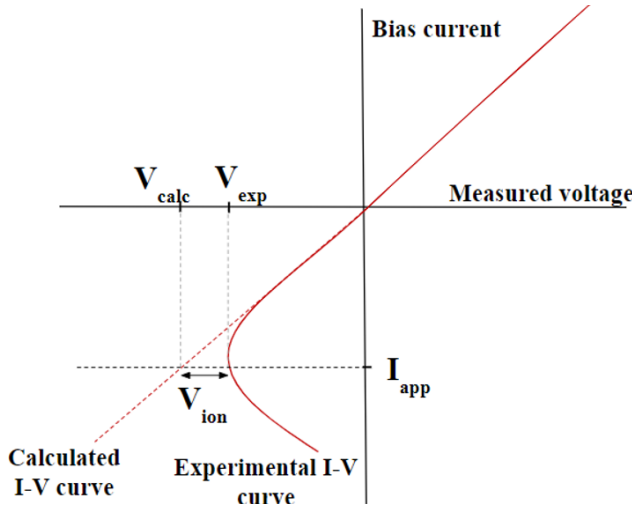


Fig. 7 For some applied current I_{app} , there are two voltage values: one which can be calculated from portion of the curve that is linear (V_{calc}) and the experimental value (V_{exp}). Any voltage difference that is the result of ion migration is the difference between these two values. In other words, $V_{ion} = V_{calc} - V_{exp}$.

Analysis

In order to gain a deeper understanding of the field-assisted ion migration potentially occurring in our samples, we focused on the c-shaped curve that was prevalent at the start of many of our measurements. This curve provided key insights into Eind. The first thing that we wanted to know was how much of the voltage drop that occurred between the voltage leads was the result of ion migration. Because E_{ion} opposes E_{bias} , we know that ion migration would cause an experimental value for V that is smaller than that which would occur

without the presence of ion migration. Each c-curve was followed by a linear section of IV curve, so we used the slope of the subsequent line to predict what the voltage drop might have been without ion migration. We then subtracted the experimental value (V_{exp}) of the voltage drop from the calculated value (V_{calc}) to get this expression for V_{ion} :

$$V_{ion} = V_{calc} - V_{exp}$$

This relationship is shown graphically in figure 7. Additionally, the calculated values for V_{ion} can be found plotted against the applied current bias for each sample in figures 9, 10, and 11.

To analyze the number and motion of the mobile ions, we simulated their movement as though all of the positive mobile ions were concentrated at one end of the sample and all of the negative mobile ions at the other end like two point charges of equal and opposite charge. We used the measured V_{ion} to calculate the total charge of each of these points, or “blobs” of accumulated ions. This setup is visualized in figure 8.

Figure 8: This image shows how the gathering of mobile ions on the sample (above) was simplified into a system of two point charges.

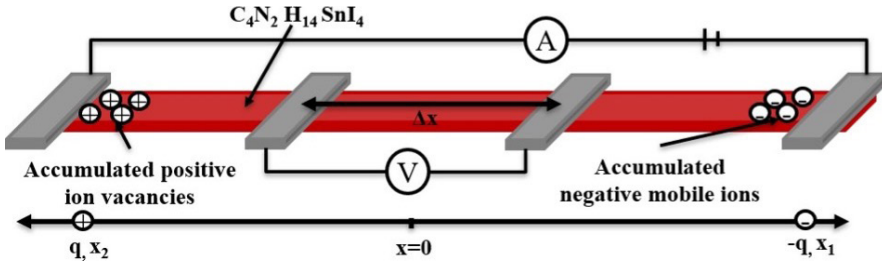


Fig. 8 The charge of each point charge, q and $-q$, are equal to the total charge of each accumulation of mobile ions. The distance of the two current leads (x_1 and x_2) from the center of the sample is the distance of the point charges from '0' on the x-axis. Δx is the distance between the two voltage leads.

In order to find charge q in terms of V_{ion} , an expression was written for difference between the potentials at each voltage lead (V_2 and V_1) from the two point charges.

$$V_{ion} = V_2 - V_1 \quad (2a)$$

$$V_1 = 1/(4\pi\epsilon_0) ((-q)/(x_1 - 1/2d) + q/(x_2 + 1/2d)) \quad (2b)$$

$$V_2 = 1/(4\pi\epsilon_0) ((-q)/(x_1 + 1/2d) + q/(x_2 - 1/2d)) \quad (2c)$$

NONLINEAR CURRENT-VOLTAGE CHARACTERISTICS

$$V_{\text{ion}} = q \Delta x / (4\pi\epsilon_0) (1/(x_1^2 - 1/4\Delta x^2) + 1/(x_2^2 - 1/4\Delta x^2)) \quad (2d)$$

Solving this equation for q gives us

$$q = (4\pi\epsilon_0) / \Delta x V_{\text{ion}} (1/(x_1^2 - 1/4\Delta x^2) + 1/(x_2^2 - 1/4\Delta x^2))^{-1} \quad (3)$$

It is now possible to calculate the number of mobile ions accumulated at each end of the sample. If our mobile ions are in fact I^- ions, then each ion has an individual charge of

$$I^- = -1 * e = -1.602 \times 10^{-19} \text{ C} \quad (4)$$

Therefore the total number of ions (n) at each end of the sample is given by

$$n = |q / (-1.602 \times 10^{-19} \text{ C})| \quad (5)$$

Calculations and analysis of the accumulation of these charges can be found in figures 9, 10, and 11.

In general, n was significantly higher at the initial maximum applied biases and decreased with the bias current. This is consistent with other findings (Wang et al., 2019), as the density of mobile ions increases with higher biases. In all three samples, whatever effect light had on the accumulated charge ions seemed to be reversible as the calculations based on data taken before light was applied and after a relaxation period were extremely similar. Additionally, the n vs I curves could be grouped into three main sections for each sample: measurements taken before and long after light was applied, measurements taken while the sample was illuminated, and the measurement taken at the moment that the light source was turned off. What was consistent across all three samples was that each group showed some pattern. Said pattern, however, was not consistent across the samples. First, we can examine sample A. Without illumination, including the measurement taken as soon as the laser was removed, n was small but positive from -30 to -20 nA bias and then became approximately zero for the rest of the measurement. Measurements taken while the sample was illuminated also saw n approach zero, but continuously saw fluctuations nearing 15×10^4 ions after that, particularly from 10 to 30 nA bias. This is consistent with our hypothesis of ion migration. With a higher bias, the number of mobile ions concentrated at each end of the sample should increase as the induced E_{ion} is proportional to applied bias. Sample C had a similar pattern, where measurements taken without the illumination saw n remain approximately zero after the initial decrease of accumulated ions, while with illumination n moved further away from zero as the positive bias increased.

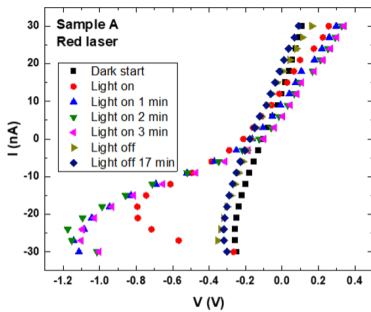
In sample B, n began with a positive accumulation that was nearly zero with -20 to 0 nA bias for all measurements. As the positive bias increased, n became non-zero and then re-approached zero when no illumination had been applied

for a while. While we were shining the laser on the sample, n moved farther and farther from zero as the positive bias current increased. For the measurement taken at the removal of light, the accumulation of ions increased to a level much higher than any of the other measurements with the application of a positive bias current. It is unclear why there is so much variation in this sample from the other two. It could be the result of the wavelength of the light source, or some factor of the sample's structure/fabrication. More research and a larger data size are needed to understand the relationship between illumination wavelength and the behavior of mobile ions.

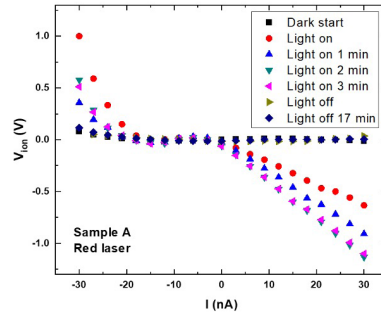
In all three samples, one thing of note is that the accumulation of mobile ions seems to be reversible. The measurements taken before any light was applied and the measurements taken after ≈ 15 minutes of relaxation time are extremely similar.

Figure 9: These figures show the data taken from sample A as it was exposed to a red laser, as well as the subsequent analysis performed on said data.

9a.



9b.



9c.

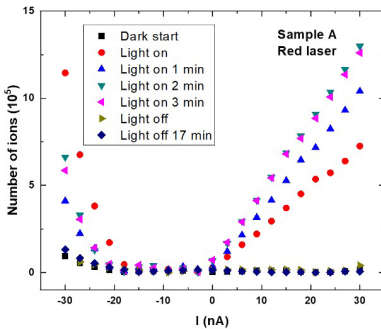


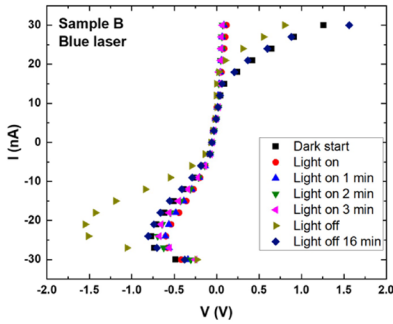
Fig. 9 Figure (a) shows the bias current vs measured voltage. These curves

NONLINEAR CURRENT-VOLTAGE CHARACTERISTICS

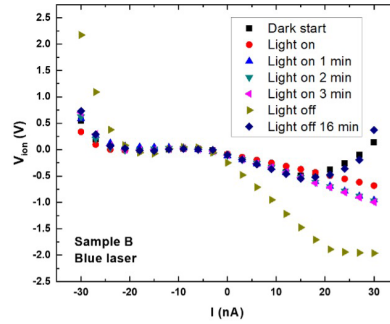
all show the characteristic C-shape at the beginning of their measurement. Measurements taken when light was not being applied develop a linear shape immediately after the C-curve. Measurements taken while the sample was illuminated have a much smaller slope until the bias reached approximately 0 nA, at which point the resistance became similar to those curves without illumination. **Figure (b)** is a plot of V_{ion} , calculated from equation (7), plotted against the bias current. **Figure (c)** shows the number of accumulated ions at each current lead, calculated from equation (5).

Figure 10: These figures show the data taken from sample B as a blue laser was shined on it, as well as the subsequent analysis.

10a.



10b.



10c.

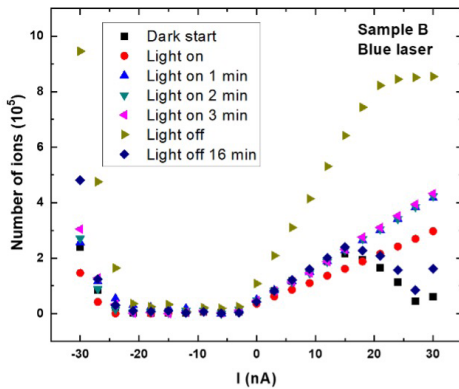
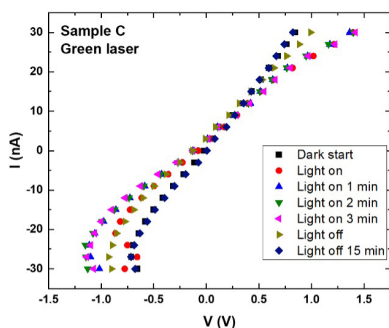


Fig. 10 **Figure (a)** shows the bias current vs measured voltage. These curves all show the characteristic C-shape at the beginning of their measurement. This C-shape exhibited little change with the application of the laser but became significantly more pronounced as soon as the laser was removed. **Figure (b)** is a plot of V_{ion} , calculated from equation (7), plotted against the bias current. **Figure**

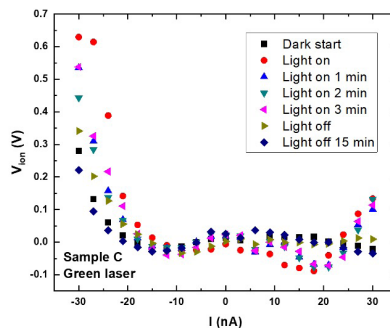
(c) shows the number of accumulated ions at each current lead, calculated from equation (5).

Figure 11: These figures show the data taken from sample C as a green laser was shined on it, as well as the subsequent analysis.

11a.



11b.



11c.

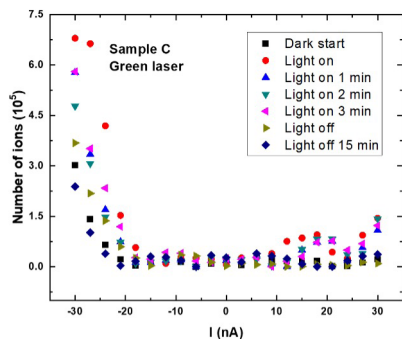


Fig. 11 Figure (a) shows the bias current vs measured voltage. These curves all show the characteristic C-shape at the beginning of their measurement. Aside from the C-shape, these curves are mostly linear. The slope of each linear line seems to decrease with the prolonged application of light, implying a decreasing resistance. Figure (b) is a plot of V_{ion} , calculated from equation (7), plotted against the bias current. Figure (c) shows the number of accumulated ions at each current lead, calculated from equation (5).

Conclusions

We performed an experiment to examine the electrical transport properties, especially the effect of photo illumination, on N,N'-dimethylethylenediaminium tin iodide ($C_4N_2H_{14}SnI_4$). This was done by monitoring the I-V curves for multiple samples before, during, and after subjecting them to a monochromatic light

NONLINEAR CURRENT-VOLTAGE CHARACTERISTICS

source.

Much of the analysis in this thesis was concentrated on the C-curves present in our I-V measurements, as well as modeling the number of accumulated mobile ions in each sample from the I-V data. Ultimately, the hypothesis that ion migration may be responsible for these C-curves was supported by our mathematical calculations. However, several I-V curves show behavior at high positive bias that mimics the negative C-curve. If it is possible that ionic current is being induced by a high negative bias, it is worth examining in future work whether or not a similar ionic movement is occurring in the opposite direction with the application of a high positive bias.

In the sample labeled A, all of the data that was collected supported the presence of ion migration, both in the negative and positive bias regions. First of all, each I-V curve showed the customary C-shape suggesting the migration of mobile ions and the accompanying electric field. The other two main areas of analysis, including the voltage drop resulting from the accumulation of mobile ions and the modeled number of mobile ions, also supported this hypothesis in both bias regions. Samples B and C mimicked some of the general behaviors of sample A with fluctuation, although sample C exhibited more of these important characteristics than B. As all three samples were taken from the same batch, it may be worthwhile in future to perform a similar experiment with many samples synthesized under the same conditions. Additionally, our modeling was based on the simplification of the two accumulated mobile ion clouds to two point charges. More specific and rigorous modeling may provide further insight.

Although our data was performed in the presence of a concentrated light source and with the hope of identifying some relationship between applied light and I-V behavior, no definitive patterns were identified that could be correlated with the wavelength of incoming excitons. Future research in this area would require a larger data pool, as these samples are not stable enough to withstand multiple runs.

References

- Andreani, L. et al. (2018). Silicon solar cells: toward the efficiency limits. *Adv. in Phys. X*, 4(1). <https://doi.org/10.1080/23746149.2018.1548305>
- Aspiroz, J. et al. (2015). Defect migration in methylammonium lead iodide and its role in perovskite solar cell operation. *Energy Environ. Sci.*, 2015(8). <https://doi.org/10.1039/C5EE01265A>
- Best Research-Cell Efficiency Chart*. (2020). National Renewable Energy Lab. <https://www.nrel.gov/pv/cell-efficiency.html>
- Eames, C., Frost, J., Barnes, P. et al. (2015). Ionic transport in hybrid lead iodide perovskite solar cells. *Nat Commun*, 6(7497). <https://doi.org/10.1038/ncomms8497>
- Editorial. (2018, March 6). *A History of Perovskite Solar Cells*. BCC Research. blog.bccresearch.com/a-history-of-perovskite-solar-cells.
- Kamminga, M. et al. (2019). Electronic mobility and crystal structures of 2,5-dimethylanilinium triiodide and tin-based organic-inorganic hybrid compounds. *J. Solid State Chem.* 270, 593-600. <https://doi.org/10.1016/j.jssc.2018.12.029>
- Lee, H. et al. (2019). Effect of Halide Ion Migration on the Electrical Properties of Methylammonium Lead Tri-Iodide Perovskite Solar Cells. *J. Phys. Chem.* 123(29), 17728–17734. <https://doi.org/10.1021/acs.jpcc.9b04662>
- Liu et al. (2019). Fundamental Understanding of Photocurrent Hysteresis in Perovskite Solar Cells. *Advanced Energy Materials*, 9(13), <https://doi.org/10.1002/aenm.201803017>
- Ma, C. et al. (2019). High performance low-dimensional perovskite solar cells based on a one dimensional lead iodide perovskite. *J. Mater. Chem. A*, 7, 8811-8817. <https://doi.org/10.1039/C9TA01859J>
- Perovskite Solar Cells*. Energy.gov. <https://www.energy.gov/eere/solar/perovskite-solar-cells>
- Vekony, A. T. (2020, December 16). *Silicon Solar Panels*. Greenmatch. <https://www.greenmatch.co.uk/solar-energy/solar-panels#how-they-work>
- Wang et al. (2017). Dynamic Electronic Junctions in Organic–Inorganic Hybrid Perovskites. *Nano Letters*, 17 (8), 4831-4839. DOI: 10.1021/acs.nanolett.7b01665
- Xia, G. et al. (2019). Nanoscale Insights into Photovoltaic Hysteresis in Triple-Cation Mixed-Halide Perovskite: Resolving the Role of Polarization and Ionic Migration. *Advanced Energy Materials*, 31(36). <https://doi.org/10.1002/adma.201902870>